bioRxiv preprint doi: https://doi.org/10.1101/2024.02.29.582786; this version posted March 27, 2024. The copyright holder for this preprint (which was not certified by peer review) is the author/funder, who has granted bioRxiv a license to display the preprint in perpetuity. It is made available under aCC-BY-NC-ND 4.0 International license.

Supplemental materials

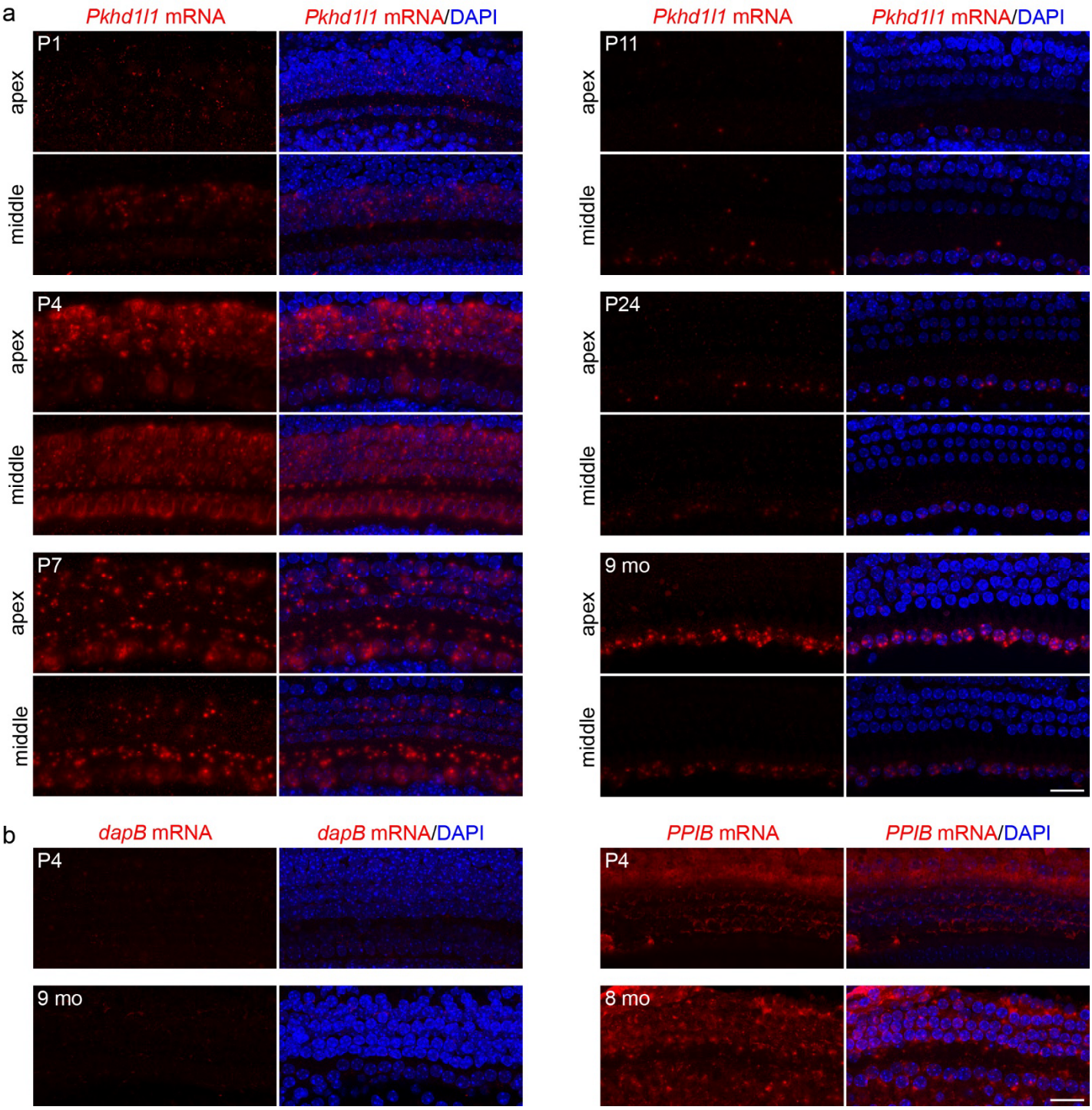

Supplemental Figure 1. *Pkhd1l1* mRNA levels in apical and mid-cochlear hair cells gradually decrease during early postnatal development. a, *In situ* detection of *Pkhd1l1* mRNA by RNAscope fluorescence labeling of the apical and mid-cochlear region reveals gradual decrease of mRNA signal in both, OHCs and IHCs by P11, while the mRNA levels in IHCs increase by 9 months. *Red*, *Pkhd1l1* mRNA fluorescence. *Blue*, DAPI. **b,** Negative control: *dapB* mRNA detection (dihydrodipicolinate reductase gene of *Bacillus subtilis*) in the mid-cochlear region shows negligible signal at P4 and 9-month time points. Positive control: *PPIB* mRNA (Cyclophilin B, ubiquitously expressed at low levels providing a rigorous control for sample quality) is detected at comparable levels in the mid-region of P4 and 8-month cochlea. *Scale bars,* 20 µm.

bioRxiv preprint doi: https://doi.org/10.1101/2024.02.29.582786; this version posted March 27, 2024. The copyright holder for this preprint (which was not certified by peer review) is the author/funder, who has granted bioRxiv a license to display the preprint in perpetuity. It is made available under aCC-BY-NC-ND 4.0 International license.

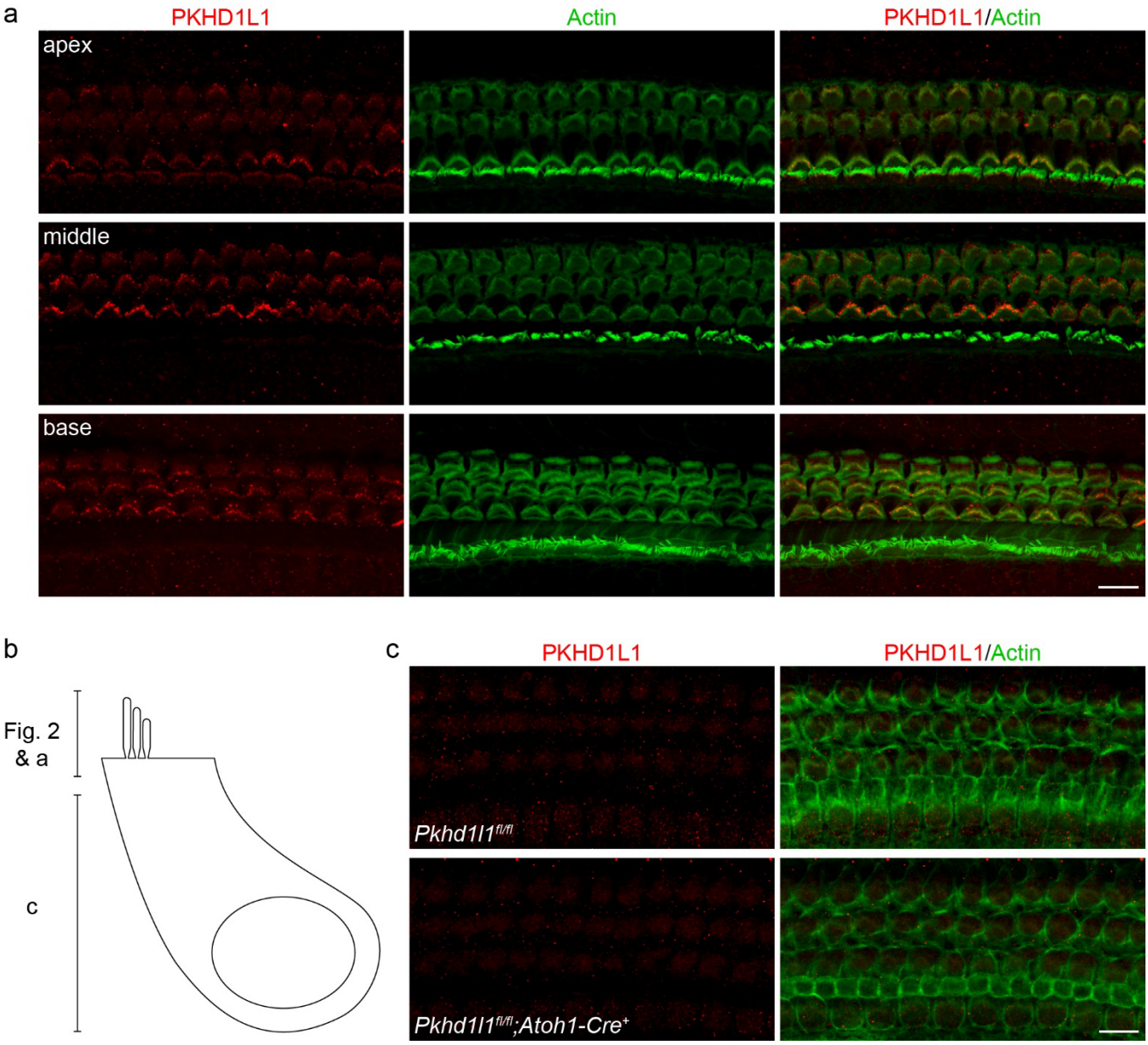

Supplemental Figure 2. **PKHD1L1 is primarily detected within hair-cell stereocilia bundles and not in cell bodies.**
a, Maximum intensity z-projection images of anti-PKHD1L1 labeling present in the hair cell stereocilia at P8 in the apex, middle and basal regions of the cochlea. **b,** Schematic of confocal z-projection depths in Figure 2 and panels a & c. **c,** Maximum intensity z-projection images of anti-PKHD1L1 labeling within the hair cell bodies at P4 in the basal region of the cochlea. No PKHD1L1-specific fluorescence is observed in normal *Pkhd1l1*$^{fl/fl}$*::Atoh1-Cre*$^{-}$ mice compared to *Pkhd1l1*$^{fl/fl}$*::Atoh1-Cre*$^{+}$ negative controls, although some non-specific labeling is present in both genotypes. *Red*, anti-PKHD1L1; *Green*, Phalloidin labeling. *Scale bars,* 10 µm.

bioRxiv preprint doi: https://doi.org/10.1101/2024.02.29.582786; this version posted March 27, 2024. The copyright holder for this preprint (which was not certified by peer review) is the author/funder, who has granted bioRxiv a license to display the preprint in perpetuity. It is made available under aCC-BY-NC-ND 4.0 International license.

858

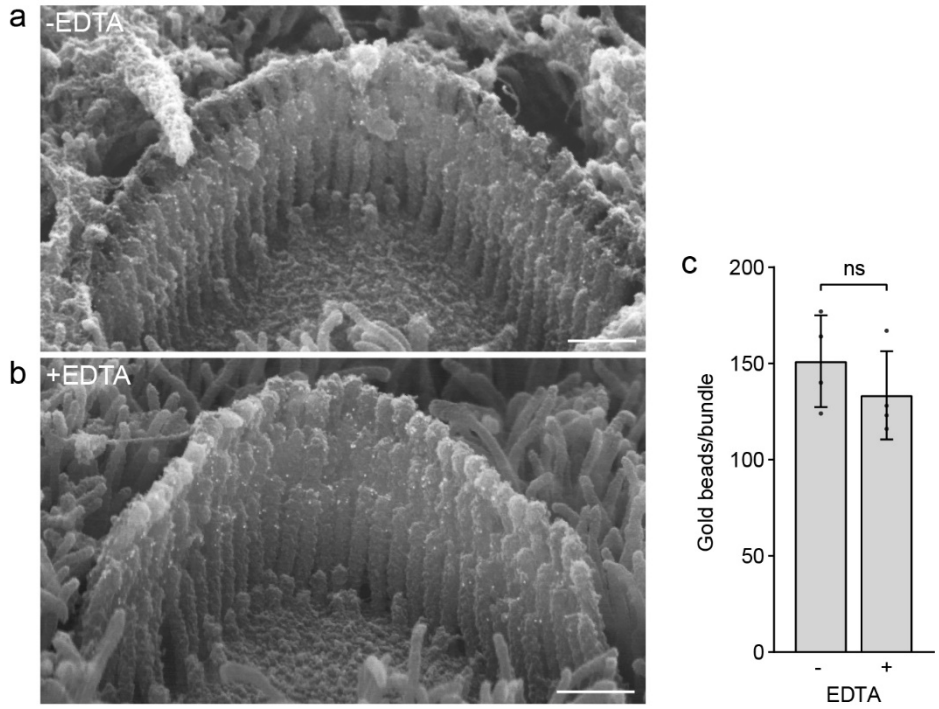

Supplemental Figure 3. **Anti-PKHD1L1 immunogold labeling efficiency is not affected by decalcification.**
a, Representative SEM images of OHC stereocilia bundle labeling of acutely fixed (*top*) and fixed then decalcified (*bottom*) cochlea. *Scale bar*, 500 nm. **b**, Quantification of gold beads per OHC stereocilia bundle. *Statistical analysis*, two-tailed t-test, p>0.05. Data displayed as mean ± SD, points represent individual cells (n=4 in each condition).

bioRxiv preprint doi: https://doi.org/10.1101/2024.02.29.582786; this version posted March 27, 2024. The copyright holder for this preprint (which was not certified by peer review) is the author/funder, who has granted bioRxiv a license to display the preprint in perpetuity. It is made available under aCC-BY-NC-ND 4.0 International license.

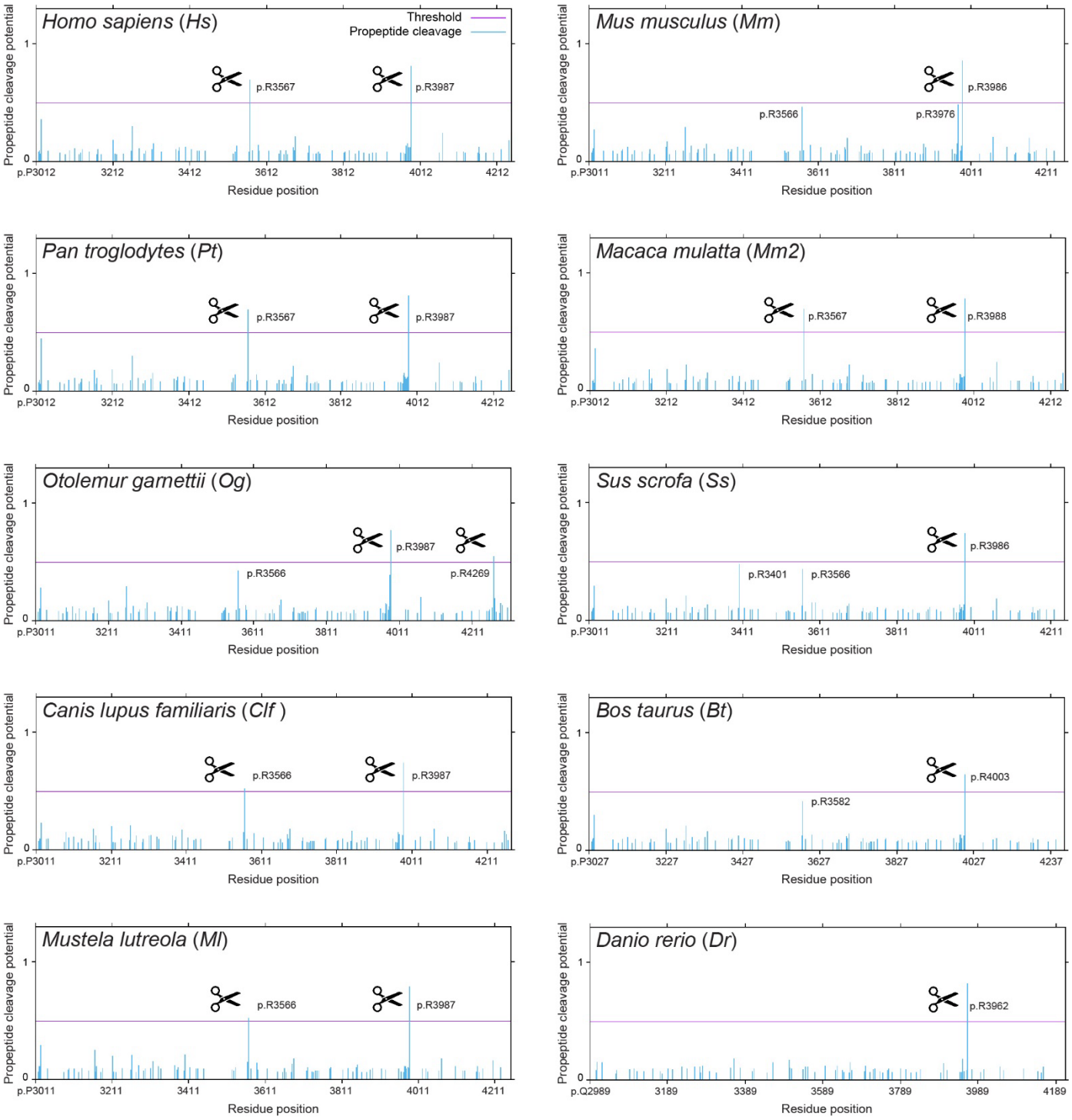

859

Supplemental Figure 4. Prediction of potential cleavage sites in PKHD1L1 proteins orthologs.

Cleavage sites were predicted across 10 different orthologs for full-length PKHD1L1 protein sequences. Only the region of each PKHD1L1 protein sequence where the cleavage sites are predicted are shown for clarity (see Sup. Table 1 for list of the species and NCBI accession codes). PKHD1L1 protein sequences were analyzed using the ProP v.1.0b ProPeptide Cleavage Site Prediction online server tool. The residue position is indicated for each species, based on NCBI accession numbers (Sup. Table S1) (X axes) and the score for each arginine (R) and lysine (K) residue is shown for the analyzed sequences (Y axes). A score of >0.5 (represented by the purple threshold line) was used to identify residues predicted to be a pro-peptide cleavage site (marked by a black scissor sign). Other plausible cleavage sites below the threshold line are also indicated by residue numbering. A higher score reflects a higher prediction confidence.

bioRxiv preprint doi: https://doi.org/10.1101/2024.02.29.582786; this version posted March 27, 2024. The copyright holder for this preprint (which was not certified by peer review) is the author/funder, who has granted bioRxiv a license to display the preprint in perpetuity. It is made available under aCC-BY-NC-ND 4.0 International license.

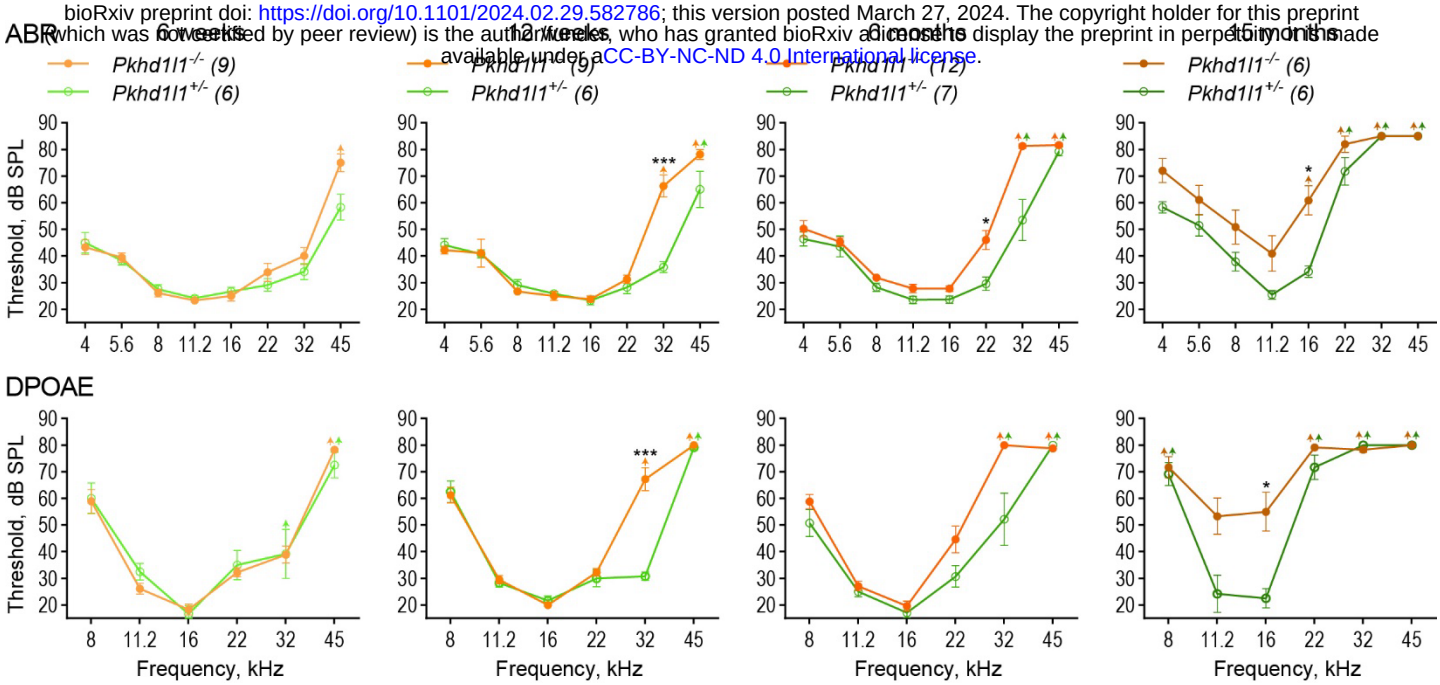

Supplemental Figure 5. *Pkhd1l1*$^{-/-}$ KO mice display progressive hearing loss.
ABR and DPOAE thresholds of constitutive *Pkhd1l1*$^{-/-}$ KO and *Pkhd1l1*$^{+/-}$ control littermate mice show progressive high-frequency hearing loss in PKHD1L1-deficient mice as early as 6 weeks. Data are shown as mean ± SEM. Up-arrows indicate that at the highest SPL level tested (80 dB SPL), at least one mouse in the group had no detectable thresholds at that frequency. *Statistical analysis*, two-way ANOVA with matched design between frequencies from the same mouse. Sidak's multiple comparison tests are shown between genotypes for each frequency. *p<0.05, **p<0.01, ***p<0.001.

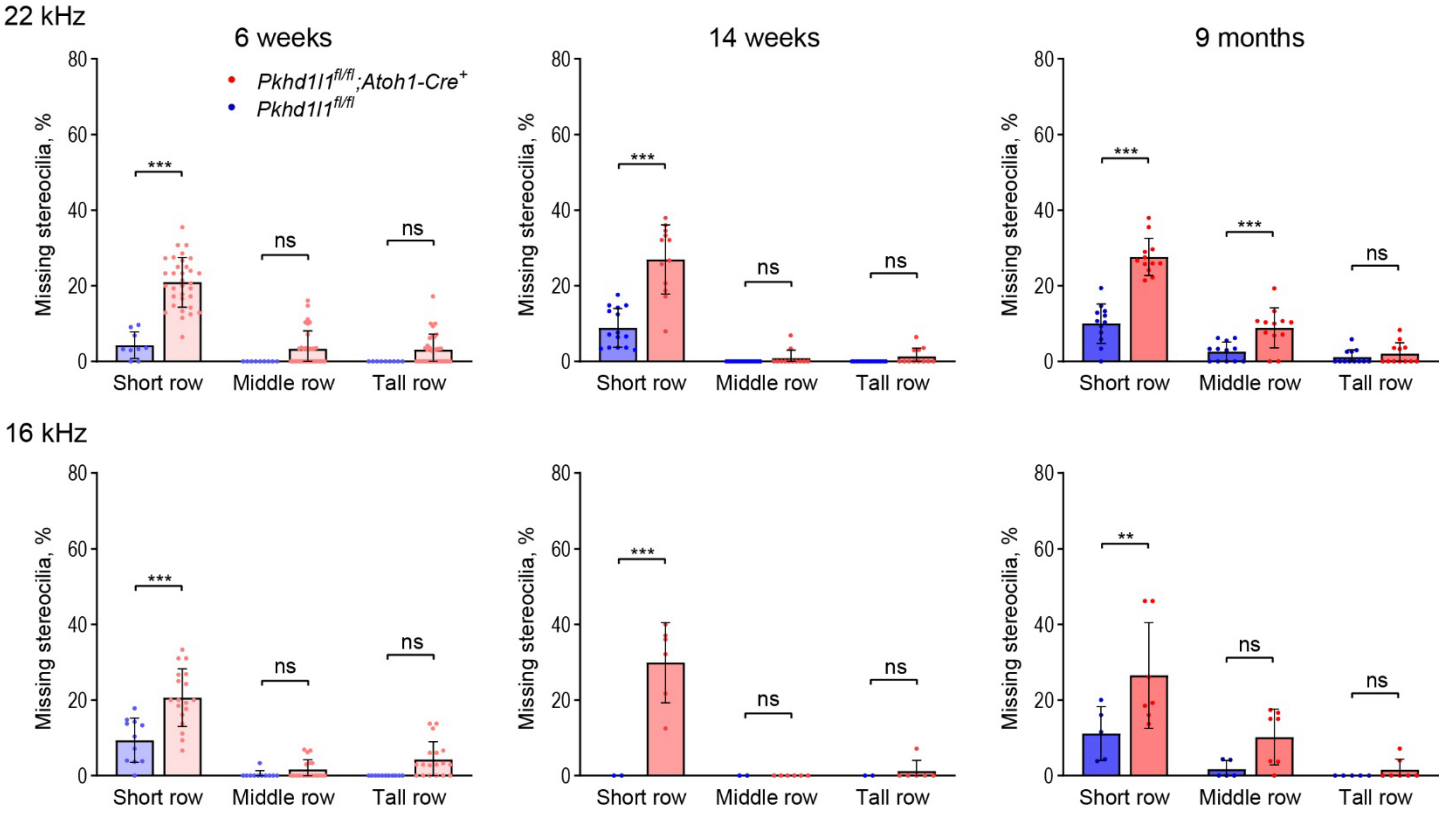

Supplemental Figure 6. Stereocilia loss in middle and apical regions of the cochlea of PKHD1L1-difficient mice.
Quantification of missing stereocilia in OHC bundles in the 22 kHz (middle) and more apical, 16 kHz, regions of the cochlea, presented as percentage of missing stereocilia, per row. There is a greater stereocilia loss in *Pkhd1l1*$^{fl/fl}$*::Atoh1-Cre*$^{+}$ mice as compared to their *Pkhd1l1*$^{fl/fl}$*::Atoh1-Cre*$^{-}$ littermates at all age points. Data displayed as mean ± SD, points represent individual cells (n numbers in methods section). *Statistical analysis*, two-way ANOVA with matched design between rows from the same cell. Sidak's multiple comparison tests are shown between rows for each genotype. *p<0.05, **p<0.01, ***p<0.001.

bioRxiv preprint doi: https://doi.org/10.1101/2024.02.29.582786; this version posted March 27, 2024. The copyright holder for this preprint (which was not certified by peer review) is the author/funder, who has granted bioRxiv a license to display the preprint in perpetuity. It is made available under aCC-BY-NC-ND 4.0 International license.

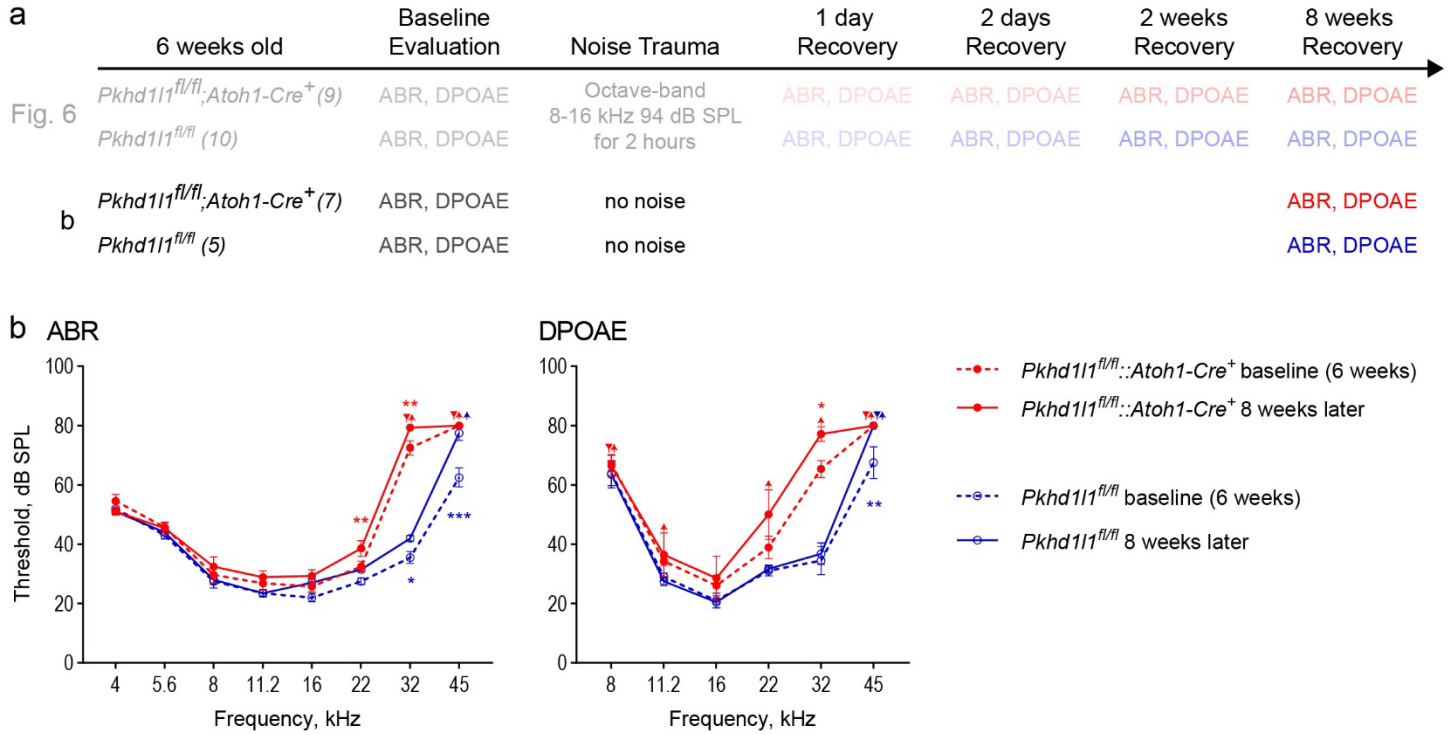

Supplemental Figure 7. Hearing performance of control mice that underwent no noise trauma exhibit detectable levels of progressive hearing loss 8 weeks later. a, Noise exposure experimental design with no noise controls. 6 week old *Pkhd1l1*$^{fl/fl}$*::Atoh1-Cre*$^{+}$ mice and *Pkhd1l1*$^{fl/fl}$*::Atoh1-Cre*$^{-}$ normal mice had baseline ABR and DPOAE evaluation prior to TTS-inducing level of noise trauma (Figure 6), or no noise trauma in controls (b). ABR and DPOAEs were recorded again 8 weeks later. **b**, ABR and DPOAE thresholds in no noise groups at 6 weeks (*dotted lines*) and 8 weeks later (*solid lines*). Both *Pkhd1l1*$^{fl/fl}$*::Atoh1-Cre*$^{-}$ control mice (*blue*) and *Pkhd1l1*$^{fl/fl}$*::Atoh1-Cre*$^{+}$ mice (*red*) show an increase in high frequency thresholds as a result of aging, in addition to the raised thresholds demonstrated in PKHD1L1-deficient mice. Data are shown as mean ± SEM. Inverted triangle (baseline) and up-arrows (8 weeks later) indicate that at the highest SPL level tested (80 dB SPL), at least one mouse in the group had no detectable thresholds at that frequency. *Statistical analysis*, two-way ANOVA with matched design between frequencies from the same mouse, and repeated measures at multiple time points. Sidak's multiple comparison tests are shown between time points for each frequency for both genotypes. *p<0.05, **p<0.01, ***p<0.001.

861

Table S1. Species and PKHD1L1 accession numbers used for multiple sequence alignment analysis, cleavage site prediction, and AlphaFold2 modelling.

Species	Abbreviation	NCBI Accession number
Homo sapiens	*Hs*	NP_803875.2
Mus musculus	*Mm*	NP_619615.2
Pan troglodytes	*Pt*	XP_016815270.3
Macaca mulatta	*Mm2*	XP_015001362.2
Otolemur garnettii	*Og*	XP_023373972.1
Sus scrofa	*Ss*	XP_020944671.1
Canis lupus familiaris	*Clf*	XP_038540795.1
Bos taurus	*Bt*	XP_024857633.1
Mustela lutreola	*Ml*	XP_059021749.1
Danio rerio	*Dr*	NP_001305057.1

bioRxiv preprint doi: https://doi.org/10.1101/2024.02.29.582786; this version posted March 27, 2024. The copyright holder for this preprint (which was not certified by peer review) is the author/funder, who has granted bioRxiv a license to display the preprint in perpetuity. It is made available under aCC-BY-NC-ND 4.0 International license.

862

Table S2. PKHD1L1 domain predictions

Consensus				Mouse UniProt				Mouse SMART				Human SMART			
Domain	Residues			Domain	Residues			Domain	Residues			Domain	Residues		
SP	1	-	20	SP	1	-	20								
IPT	31	-	132	IPT	31	-	132	IPT	30	-	141	IPT	30		130
IPT	146	-	255	IPT	146	-	255					IPT	145	-	257
IPT	270	-	361	IPT	270	-	361	IPT	269	-	362	IPT	271	-	362
PbH1	398	-	420	PA14	337	-	492	PbH1	398	-	420	PbH1	398	-	420
IPT	1067	-	1153	IPT	1067	-	1153	IPT	1066	-	1154	IPT	1066	-	1152
IPT	1155	-	1234	IPT	1155	-	1234	IPT	1156	-	1235	IPT	1154	-	1235
IPT	1240	-	1323	IPT	1240	-	1323					IPT	1239	-	1327
IPT	1329	-	1468	IPT	1329	-	1468	IPT	1328	-	1407	IPT	1329	-	1408
IPT	1565	-	1648	IPT	1565	-	1648					IPT	1565	-	1650
IPT	1658	-	1742	IPT	1658	-	1742	IPT	1657	-	1743	IPT	1658	-	1744
IPT	1748	-	1827	IPT	1748	-	1827					IPT	1748	-	1829
IPT	1830	-	1909	IPT	1830	-	1909	IPT	1829	-	1910	IPT	1830	-	1911
IPT	1915	-	1996	IPT	1915	-	1996	IPT	1914	-	1997	IPT	1915	-	1998
IPT	1998	-	2084	IPT	1998	-	2084	IPT	1998	-	2085	IPT	1999	-	2086
IPT	2090	-	2175	IPT	2090	-	2175	IPT	2089	-	2176	IPT	2090	-	2177
								PbH1	2105	-	2126				
G8	2183	-	2303	G8	2183	-	2303	G8	2183	-	2303	G8	2184	-	2304
PbH1	2484	-	2506	PbH1	2484	-	2506	PbH1	2484	-	2506				
PbH1	2507	-	2529	PbH1	2507	-	2529	PbH1	2507	-	2529	PbH1	2508	-	2530
PbH1	2565	-	2587	PbH1	2565	-	2587	PbH1	2565	-	2587	PbH1	2566	-	2588
PbH1	2664	-	2686	PbH1	2664	-	2686	PbH1	2664	-	2686	PbH1	2665	-	2687
PbH1	2732	-	2755	PbH1	2732	-	2755	PbH1	2732	-	2755	PbH1	2733	-	2756
G8	3035	-	3173	G8	3035	-	3173	G8	3035	-	3173	G8	3036	-	3174
PbH1	3292	-	3314	PbH1	3292	-	3314	PbH1	3292	-	3314	PbH1	3293	-	3315
PbH1	3354	-	3376					PbH1	3354	-	3376	PbH1	3355	-	3377
PbH1	3415	-	3437	PbH1	3415	-	3437	PbH1	3415	-	3437	PbH1	3416	-	3438
PbH1	3470	-	3492	PbH1	3470	-	3492	PbH1	3470	-	3492	PbH1	3471	-	3493
PbH1	3493	-	3514	PbH1	3493	-	3514	PbH1	3493	-	3514	PbH1	3527	-	3548
TM	4223	-	4243	TM	4223	-	4243								

863